Check for updates

AGU ADVANCING EARTH AND SPACE SCIENCE

Geophysical Research Letters

RESEARCH LETTER
10.1029/2020GL089425

Full-Depth Global Estimates of Ocean Mesoscale Eddy Mixing From Observations and Theory

Sjoerd Groeskamp[1], Joseph H. LaCasce[2], Trevor J. McDougall[3], and Marine Rogé[4]

[1]NIOZ Royal Netherlands Institute for Sea Research, Texel, Netherlands, [2]Department of Geosciences, University of Oslo, Oslo, Norway, [3]School of Mathematics and Statistics, University of New South Wales, Sydney, New South Wales, Australia, [4]Climate Change Research Centre, University of New South Wales, Sydney, New South Wales, Australia

Key Points:
- We present a new parameterization for mesoscale eddy mixing that combines mixing-length and flow-suppression theory with vertical modes
- Global, full-depth mesoscale eddy mixing estimates are obtained from observations of temperature, salinity, pressure, and eddy kinetic energy
- Mesoscale eddy mixing is surface intensified and strongly influenced by the vertical stratification of ocean density

Correspondence to:
S. Groeskamp,
sjoerdgroeskamp@gmail.com

Citation:
Groeskamp, S., LaCasce, J. H., McDougall, T. J., & Rogé, M. (2020). Full-depth global estimates of ocean mesoscale eddy mixing from observations and theory. *Geophysical Research Letters*, *47*, e2020GL089425. https://doi.org/10.1029/2020GL089425

Received 26 JUN 2020
Accepted 1 SEP 2020
Accepted article online 9 SEP 2020

Abstract Mixing by mesoscale eddies profoundly impacts climate and ecosystems by redistributing and storing dissolved tracers such as heat and carbon. Eddy mixing is parameterized in most numerical models of the ocean and climate. To reduce known sensitivity to such parameterizations, observational estimates of mixing are needed. However, logistical and technological limitations obstruct our ability to measure global time-varying mixing rates. Here, we extend mixing length theory with mean-flow suppression theory, and first surface modes, to estimate mixing from readily available observational-based climatological data, of salinity, temperature, pressure, and eddy kinetic energy at the sea surface. The resulting full-depth global maps of eddy mixing can reproduce the few available direct estimates and confirm the importance of mean-flow suppression of mixing. The results also emphasize the significant effect of eddy surface intensification and its relation to the vertical density stratification. These new insights in mixing dynamics will improve future mesoscale eddy mixing parameterizations.

Plain Language Summary Large whirls of hundreds of kilometers can mix water with different temperatures, salinity, and other properties. These whirls are called mesoscale eddies and are very difficult to include in numerical simulation of ocean and climate. Therefore, we include them using a simplified representation: a parameterization. These parameterizations need as input, the strength with which these eddies mix. Ideally, we would thus measure these mixing strengths globally and over the full depth of the ocean. However, this is impossible due to technological, logistical, and financial limitations. To avoid these limitations, we instead indirectly estimate mixing from variables that we can measure globally over the full depth of the ocean. We here present a new way to indirectly estimate mixing from widely available observations of temperature, salinity, pressure, and surface eddy kinetic energy. This results in three-dimensional maps of eddy mixing strengths. We find that eddies mix much stronger near the surface than in the deep ocean and that this is partly caused by the vertical stratification of ocean density. These new insights and maps can be used to improve mixing parameterizations and thus significantly improve all kinds of calculations that are important for the Earth's climate and ecosystems.

1. Introduction

Instability of the large-scale density field produces geostrophically balanced, mesoscale ocean eddies (Gill et al., 1974; Wunsch & Ferrari, 2004), which are central for ocean mass and tracer transport (Busecke & Abernathey, 2019; Busecke et al., 2014; Gnanadesikan et al., 2015; Jones & Abernathey, 2019). The eddies vary in size from kilometers to hundreds of kilometers and as such are unresolved in many global ocean and climate models (Chelton et al., 1998). The eddies are accordingly parameterized in the models (Fox-Kemper et al., 2019; Hallberg, 2013; Jansen et al., 2019; Meijers, 2014). But the simulations are often sensitive to the choice of parameterizations (Ferreira et al., 2005; Jones & Abernathey, 2019; Pradal & Gnanadesikan, 2014; Sijp et al., 2006).

Having proper three-dimensional observations of eddy mixing would greatly aid in the choice of parameterizations, reducing model uncertainty. Direct observations have been made in tracer release experiments (Ledwell et al., 1993, 1998) and also estimated using Lagrangian drifters and subsurface floats (LaCasce et al., 2014; Roach et al., 2018; Zhurbas & Oh, 2004), satellite data (Abernathey & Marshall, 2013; Busecke & Abernathey, 2019; Holloway, 1986; Klocker & Abernathey, 2013), hydrographic data

©2020. American Geophysical Union. All Rights Reserved.

(Chapman & Sallée, 2017), inverse methods (Groeskamp et al., 2017; Hautala, 2018; Zika et al., 2010), and salinity anomalies (Cole et al., 2015). These studies have significantly increased our understanding of eddy size, eddy kinetic energy (EKE), and mixing suppression by mean flows. Broadly speaking, the studies indicate enhanced mixing near western boundary currents and the Antarctic Circumpolar Current, and reduced mixing in the eastern subtropical gyres and at high latitudes. However, almost none of these observational-based studies offer global and/or full-depth coverage; rather, they are local, confined to the surface, or limited to the area significantly sampled by Argo floats. The one global study that we know of provides only estimates integrated over the mixed layer and the abyss (Groeskamp et al., 2017).

Here we propose a method to estimate eddy mixing using satellite observations and readily available observations of absolute salinity S_A, conservative temperature Θ, pressure p, and the surface EKE. This involves projecting the surface velocities to depth using recently derived vertical structure functions. The resulting global, full-depth diffusivity maps agree well with previous observations and indirect estimates. The vertical density stratification (N^2) dictates the extent of surface intensification of eddy mixing and, in turn, of mixing at depth. These new insights will aid the next steps in understanding, constructing, and constraining eddy mixing parameterizations.

2. The Eddy Diffusivity Parameterizations

We here study the mixing by along-isopycnal diffusion of passive tracers by mesoscale eddies, which we represent with a turbulent isopycnal mesoscale eddy diffusivity K. The foundation is an estimate based on mixing length theory (Prandtl, 1925):

$$K_{\mathrm{MLT}} = \Gamma u_{\mathrm{rms}} L_{\mathrm{mix}}. \tag{1}$$

Here Γ is the mixing efficiency, u_{rms} the rms geostrophic velocity, and L_{mix} the mixing length scale. Such a relation has been used for both atmospheric (Bretherton, 1966) and oceanic modeling (Abernathey & Marshall, 2013; Holloway, 1986; Klocker & Abernathey, 2013; Marshall & Adcroft, 2010; Naveira Garabato et al., 2015). Following the realization that mixing is suppressed in the presence of a mean flow, the above estimate was modified. For the case of a zonal mean flow, this is (Ferrari & Nikurashin, 2010; Klocker et al., 2012):

$$K = \frac{K_{\mathrm{MLT}}}{1 + k^2\gamma^{-2}\left(c_w - U\right)^2}. \tag{2}$$

Here γ is the reciprocal of an eddy decorrelation time (s^{-1}), k the zonal (eddy) wave number, c_w an eddy drift speed, and U the mean velocity.

2.1. Depth Dependent K_{MLT}

Equation 2 has been applied previously at the sea surface (Klocker & Abernathey, 2013), but here we extend it to depth by using the depth-dependent velocity $U = U(z)$ in the denominator (Ferrari & Nikurashin, 2010; Klocker et al., 2012). The velocity can be obtained from integrating the thermal wind relation downward from the sea surface. K_{MLT} also depends on depth, through its dependence on u_{rms}. Assuming the vertical structure is separable, the components of the eddy velocity can be expressed as $(u', v') = \phi(z)(u'_0, v'_0)$, where $\phi(z)$ is a vertical structure function and the zero subscript velocities are the surface values. The $u_{\mathrm{rms}}(z)$ is then given by

$$u_{\mathrm{rms}} = \sqrt{\left(u'^2 + v'^2\right)} = \phi(z)\sqrt{2\mathrm{EKE}_0}, \tag{3}$$

which can be obtained from the surface EKE_0.

The function $\phi(z)$ in turn can be found by solving a vertical structure equation, which has the vertical stratification N^2 as the only input (Charney, 1971; Gill, 1982; Wunsch, 2015). The resulting eigenmodes (the "baroclinic modes") were traditionally found assuming a flat bottom boundary. The first baroclinic mode is familiar in oceanography, having opposed flow at the surface and bottom. However, observations from current meters suggest that bathymetry affects time-dependent motion throughout the water column, in most regions of the ocean (de La Lama et al., 2016). This can be taken into account by imposing a no horizontal flow condition at the bottom, that is, $\phi(z = -H) = 0$ (Aoki et al., 2009; Hunt et al., 2012; LaCasce, 2017; Wortham & Wunsch, 2014). The gravest resulting ϕ (the "first surface mode") closely resembles the gravest empirical orthogonal function (EOF) from the current meter observations (de La Lama et al., 2016;

LaCasce & Groeskamp, 2020). The latter accounts for more than 50% of the variance in many locations. Thus, we use the first surface mode to represent the dominant vertical structure of the horizontal geostrophic eddies (Appendix B).

Bottom-trapped (topographic wave) modes (Rhines, 1970; Thompson & Luyten, 1976) may also contribute significantly to subsurface mixing. Such modes have a maximum near the bottom that decays with height, and the associated mixing would be similarly bottom intensified. However, it is presently unknown how to estimate the topographic wave field from surface data (or if that is even possible). This is should be the subject of future work.

We must also specify the mixing length, L_{mix} (Equation 1). A consistent choice is the first Rossby radius of deformation, L_{d}, the eigenvalue associated with the first baroclinic mode. Ocean eddies propagate westward, in most regions outside of the Southern Ocean (where, due to advection by the Antarctic Circumpolar Current, they drift eastward instead) (Chelton & Schlax, 1996; Chelton et al., 1998). The propagation speed is consistent with that of long Rossby waves, if one uses the deformation radius associated with the first surface mode (LaCasce & Groeskamp, 2020). As such, the surface mode radius is a reasonable choice for eddy scale.

The radius, which is inversely proportional to the Coriolis parameter, becomes infinite at the equator. Thus, one uses an alternate estimate, based on the "equatorial beta plane," at low latitudes (Chelton et al., 1998). Specifically, we use the expression of Hallberg (2013):

$$L_{\text{d}} = \frac{c_1}{\sqrt{f^2 + 2c_1\beta}}, \tag{4}$$

where c_1 is the first surface mode gravity wave phase speed, f is the Coriolis parameter, and $\beta = df/dy$ is its latitudinal gradient.

2.2. The Suppression Factor

Estimates of c_w (Equation 2) are often made using Hovmller diagrams of the sea surface height. Instead, we exploit the fact that over most of the ocean eddy drift speeds are well approximated by the surface mode phase speed, Doppler shifted by the time- and depth-averaged velocity (Chapman & Sallée, 2017; Klocker & Abernathey, 2013; Klocker & Marshall, 2014). This yields $\mathbf{c_w}(x, y) = \left(\bar{U}^{z,t} - \beta L_{\text{d}}^2, \bar{V}^{z,t}\right)$. Again, the velocities U and V are obtained from thermal wind, and L_{d} is the first surface radius. An alternate expression can be obtained assuming a two layer ocean (Wang et al., 2016), but the present version is more appropriate with continuous stratification. Finally, we write the wave number as $k = 2\pi/L_{\text{d}}$. Taken together, this yields

$$K = \underbrace{\Gamma\,\phi(z)\sqrt{2\text{EKE}_0}\,L_{\text{d}}}_{K_{\text{MLT}}} \times \min\left(S^x, S^y\right), \tag{5}$$

with

$$S_x = \frac{1}{1 + \frac{4\pi^2}{\gamma^2 L_{\text{d}}^2}(\delta v)^2}, S_y = \frac{1}{1 + \frac{4\pi^2}{\gamma^2 L_{\text{d}}^2}\left(\delta u - \beta L_{\text{d}}^2\right)^2}, \tag{6}$$

where $\delta v = \bar{v}^{z,t} - v(z)$ and $\delta u = \bar{u}^{z,t} - u(z)$. Note that U_0 and V_0 have canceled out, avoiding the introduction of errors through an estimate of the surface velocity. As such, δu and δv are entirely determined from hydrography, $\left(S_{\text{A}}, \Theta, p\right)$.

Suppression theory provides a means for estimating cross-stream diffusivities, as along-stream transport is dominated by advection (Ferrari & Nikurashin, 2010). Following Chapman and Sallée (2017) and Klocker and Abernathey (2013), we use the minimum suppression factor, that is, $\min\left(S^x, S^y\right)$, rather than the value perpendicular to the large-scale mean flow (Zhurbas & Oh, 2004). The latter was attempted but yielded noisier results due to uncertainties in the rotation angle. Finally, we note that γ is used as a fitting parameter, as discussed later.

3. Collecting the Ingredients

Thus, we require only observations of S_{A}, Θ, p, and EKE_0 to calculate K. The former were obtained from annual mean fields from the World Ocean Atlas 2018 (Garcia et al., 2019), gridded climatology, while the EKE_0 comes from CMEMS (Copernicus Marine Environment Monitoring Service) operational delayed-time sea surface geostrophic velocity anomalies derived from satellite altimetry (Pujol et al., 2016; Taburet et al., 2019) (Appendix A). The mixing parameter was set to be $\Gamma = 0.35$ (Klocker & Abernathey, 2013).

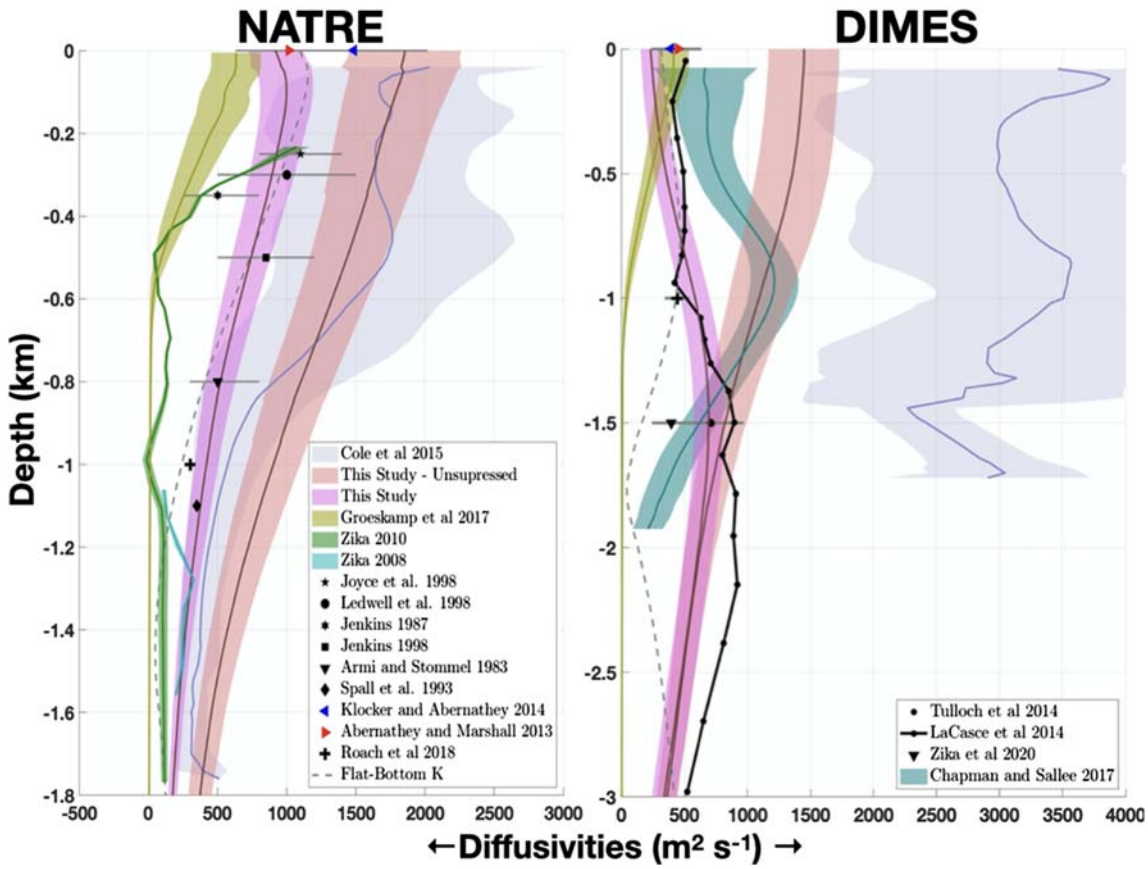

Figure 1. Comparing the present results against direct observations (black points) (Armi & Stommel, 1983; Jenkins, 1987, 1998; Joyce et al., 1998; Ledwell et al., 1998; Spall et al., 1993; Tulloch et al., 2014; Zika et al., 2020) and indirect estimates (Abernathey & Marshall, 2013; Chapman & Sallée, 2017; Cole et al., 2015; Groeskamp et al., 2017; Klocker & Abernathey, 2013; LaCasce et al., 2014; Roach et al., 2018; Zika et al., 2010; Zika & McDougall, 2008) in the NATRE (left) and DIMES (right) region.

The decay rate, γ, was obtained by fitting K to the diffusivity estimates obtained from the North Atlantic Tracer Release Experiment (NATRE) and Diapycnal and Isopycnal Mixing Experiment in the Southern Ocean (DIMES). The parameter was found via a least squares fit using both sets of data (using only estimates indicated with black colors in Figure 1). We find $\gamma^{-1} = 1.68$ days, which is comparable to, but also somewhat smaller than the 4 days found previously for the surface (Klocker & Abernathey, 2013).

4. Comparing to Observations

The resulting diffusivity profiles compare well to those obtained in NATRE and DIMES (Figure 1). The present estimate captures the vertical decay in the NATRE profile, and also the subsurface maximum observed in the DIMES experiment. Notably, in both cases including the mean flow suppression factor significantly improves the results.

Other estimates are also shown for comparison. The semiglobal estimates of Cole et al. (2015) somewhat overestimate the diffusivities, while the global inverse estimates of Groeskamp et al. (2017) underestimate them. An additional curve is included in each case showing the vertical structure if the traditional (flat-bottom) baroclinic mode is used instead of the surface mode (Appendix B). This yields a middepth minimum and thus a very different vertical structure than observed.

4.1. Global Maps

The factor indicating mean flow suppression of the mixing, given in (6), is mapped in Figure 2. Suppression is enhanced in the cores of the western boundary currents and reduced on their flanks. It is pronounced in the Antarctic Circumpolar Current, over large swaths of the Southern Ocean. Suppression is also strongly

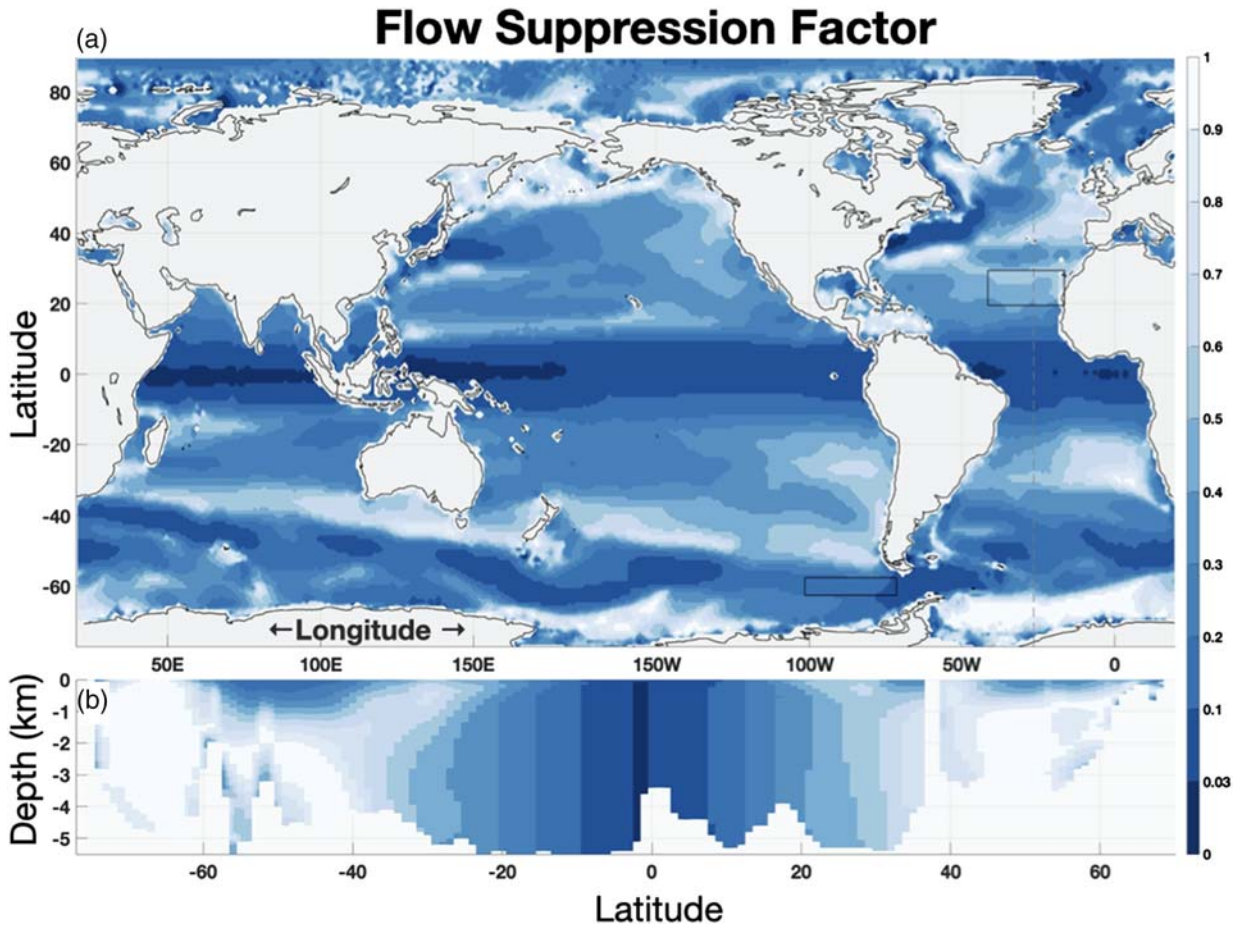

Figure 2. The suppression factor at the surface (Equation 6) (a) and for a north-south transect in the Atlantic ocean (b), as indicated by the meridional gray dashed line in (a). NATRE and DIMES are indicated by squares.

evident at low latitudes, reflecting the large deformation radius there. Suppression is correspondingly weaker in the high latitudes, where L_d is small.

The suppression factor helps understand the spatial variability exhibited by the diffusivity, shown in Figure 3. For example, K is weaker in the core of the Gulf Stream but enhanced to its south, while diffusivities in the equatorial region are smaller than in the subtropical gyres. Diffusivities are large in the Agulhas system, in the South Equatorial Current in the Indian Ocean and in the western Pacific. Yet diffusivities are smaller at high latitudes, as the smaller L_d yields a shorter mixing length. Previously noted features such as the mixing desert in the North Pacific and Subtropical Southern Atlantic (Abernathey & Marshall, 2013; Klocker & Abernathey, 2013) are also clearly seen. Meanwhile, the estimates in the NATRE and DIMES regions, indicated by the squares in the eastern North Atlantic and the South Pacific, respectively, compare well to those described previously (Abernathey & Marshall, 2013; Chapman & Sallée, 2017; Klocker & Abernathey, 2013) (Figure 1).

Mean flow suppression also varies with depth (Figure 2b), affecting the vertical structure of the diffusivities (Figure 3b). Strong suppression is observed at all depths in the tropics, but suppression is intensified near the surface and weaker at depth at midlatitudes. It is for this reason the diffusivity exhibits a subsurface maximum in for example the Southern Ocean (Figure 3b), including the DIMES region (Figure 1) (Abernathey et al., 2010; Klocker et al., 2012; LaCasce et al., 2014; Tulloch et al., 2014).

The vertical variation of the diffusivity also depends on the vertical structure of the EKE, represented by the function $\phi(z)$. As noted, this is obtained by applying theoretical arguments to an observationally based gridded hydrographic climatology (LaCasce & Groeskamp, 2020). We illustrate this by mapping the depth at which ϕ has decreased by an e-folding scale from its surface value ($\phi(z) = 1/e = 0.37$; Figure 4a) and

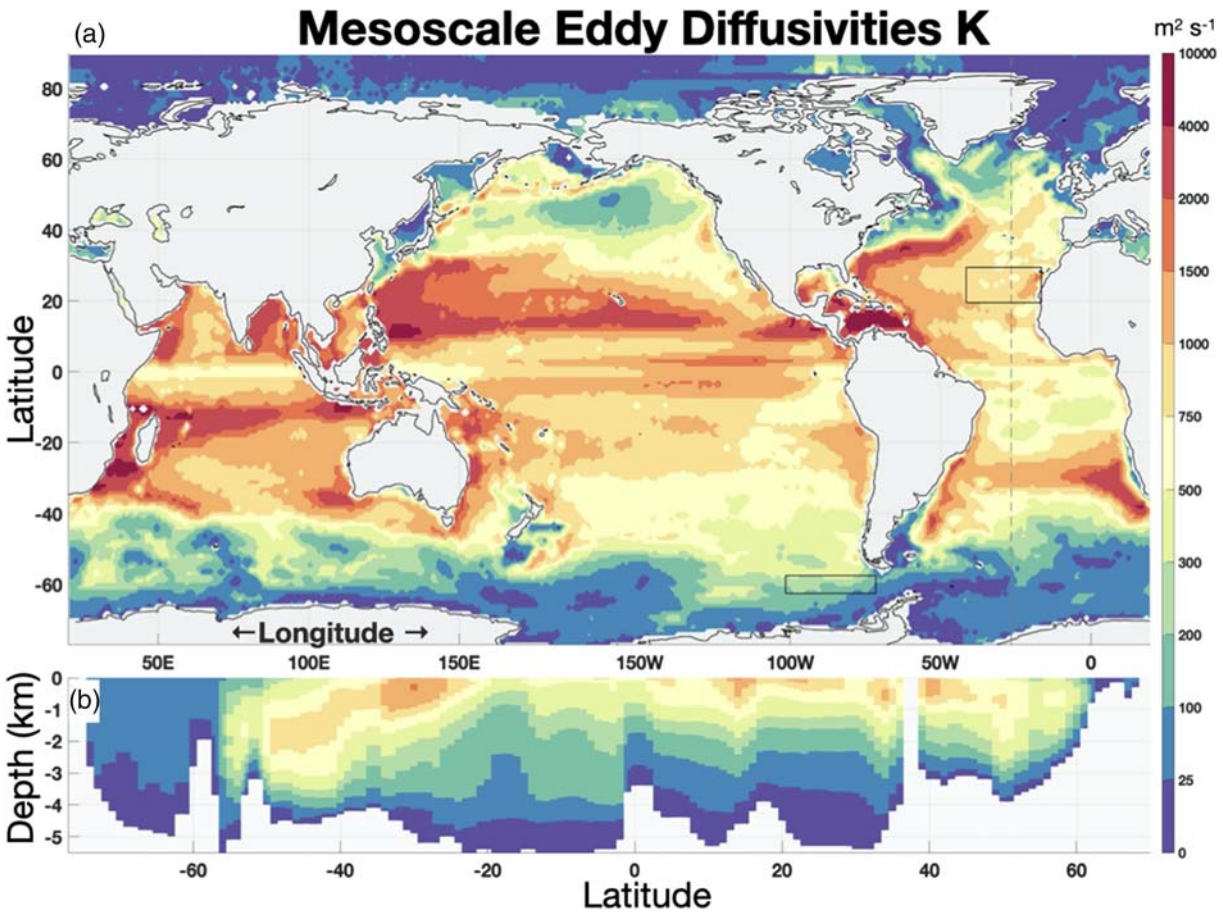

Figure 3. The diffusivity K at the ocean surface (a) and for a north-south transect in the Atlantic ocean (b) along the gray dashed line in (a). The NATRE and DIMES regions are indicated by rectangles.

show representative vertical profiles of $\phi(z)$ (Figure 4b). The e-folding depth is small in shallow regions, for instance along the continental slopes. It is large where the stratification is weak, notably near Antarctica and in the Labrador Sea, and smaller where the stratification is strong, as in the subtropical gyres (10–30°N and 10–30°S). That the diffusivity is strongly surface intensified is also clear in the NATRE region (Figure 1).

There is significant longitudinal variation, however, for example, in the South Atlantic. The larger e-folding depth in the west stems from the intrusion of Antarctic Bottom Water. This increases the deep ocean stratification, causing a more gradual vertical decay of ϕ (to satisfy the bottom boundary condition) than in the east side of the basin. This contrast is consistent with data from two WOCE current meters, at the locations indicated by the star and diamond in the map. The first EOFs, derived from the horizontal velocities (Figure 4b), are plotted in the insert. The eastern current meter (though just to the east of the shallow portion of the map) has an EOF that decays more rapidly with depth that the western current meter (the starred profile). This leads to stronger surface intensification in the east and thus larger mixing rates at depth in the western South Atlantic than in the east.

5. Summary

A new parametrization for the along-isopycnal mesoscale eddy diffusivity is presented. This novelly extends the Prandtl (1925) mixing length theory employing mean-flow suppression theory (Ferrari & Nikurashin, 2010) and the theory of vertical modes over bathymetry (LaCasce & Groeskamp, 2020). The parameterization is applied to widely and readily available observations of S_A, Θ, p, and surface EKE to produce a global, full-depth map of along-isopycnal mesoscale eddy diffusivity. The estimated diffusivities exhibit strong spatial variations and are in line with previous surface estimates and also agree well with subsurface profiles obtained from experiments in the eastern North Atlantic and the Southern Ocean.

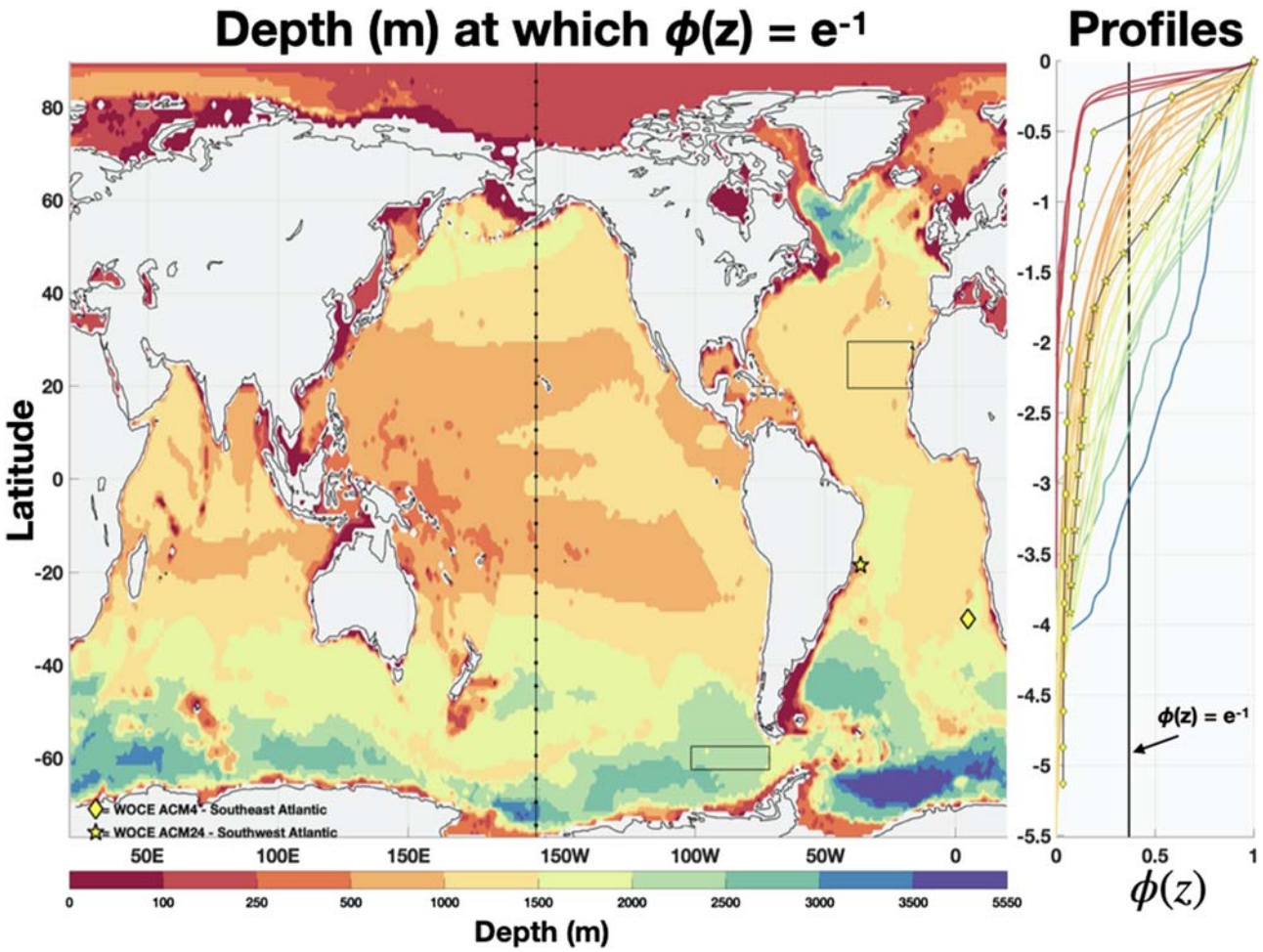

Figure 4. The e-folding depth for the geostrophic eddy velocity, that is, the depth at which $\phi(z) = 0.37$ (left). The star and diamond indicate the locations of the ACM24 (Durrieu De Madron & Weatherly, 1994) and ACM04 (Garzoli et al., 1996) current meter moorings, respectively. Examples of individual profiles of $\phi(z)$ (right). The profiles are from 160° W, indicated by the black dotted line in the left panel, and the two current meters. The colors are the same as for the left panel.

The adopted surface mode vertical structure, while supported by observations, has not yet been widely adopted (Stanley et al., 2020). An exception is the Geophysical Fluid Dynamics Laboratory (GFDL) OM4.0 numerical model, which employs a first baroclinic mode with no slip imposed at the bottom when representing the vertical structure of the diffusivity (Adcroft et al., 2019). With strong surface stratification, relative to the abyssal stratification, the surface mode is strongly surface intensified. This is in line with previous studies that also found indications of surface intensification (Canuto et al., 2019; Groeskamp et al., 2017). Consequently, large-scale thermohaline and wind forcing that alters surface stratification determine how mixing varies with depth. Thus while eddies may alter the stratification (Dewar, 1986), stratification also impacts eddy mixing.

The diffusivities derived here represent mesoscale mixing of tracer (Redi, 1982), yet the same eddies also mix mass between pairs of density surfaces. This is called the temporal residual-mean velocity in height-coordinate models and bolus velocity in density coordinate models (McDougall & McIntosh, 2001). The tracer and "mass" diffusivities are known to differ but are related through theoretical considerations as described by Smith and Marshall (2009). Applying their theory to the presented diffusivities may provide a way forward to use the results of this study for both temporal residual-mean and bolus-velocity transports.

The development of mixing parameterizations that are able to respond to changing state of the ocean remains a challenge for numerical modeling (Fox-Kemper et al., 2019). The present parameterization, based on the ocean state, provides a way forward to overcome this challenge. This will in turn much improve numerical modeling of ocean physics, biogeochemistry, and future climate.

Appendix A: The Data

World Ocean Atlas in situ temperature and practical salinity are used to calculate conservative temperature Θ and absolute salinity S_A (Graham & McDougall, 2013; IOC et al., 2010; McDougall, 2003; McDougall et al., 2012) using the GSW software toolbox (McDougall & Barker, 2011) and are then interpolated to a 10 m vertical grid resolution using interpolation software of Barker and McDougall (2020). The resulting data are made statically stable using Barker and McDougall (2017), with a minimum stability given by Jackett and McDougall (1997). The resulting buoyancy frequency N^2 is smoothed with a 5-point running mean to filter out small-scale oscillations.

The CMEMS multiple-satellite-merged data are daily, spanning from 1993 to present, and gridded at a spatial resolution of 0.25° in both zonal and meridional directions. The geostrophic currents are calculated using the geostrophic relations for latitudes outside the ±5° N band, and using a β-plane approximation of the

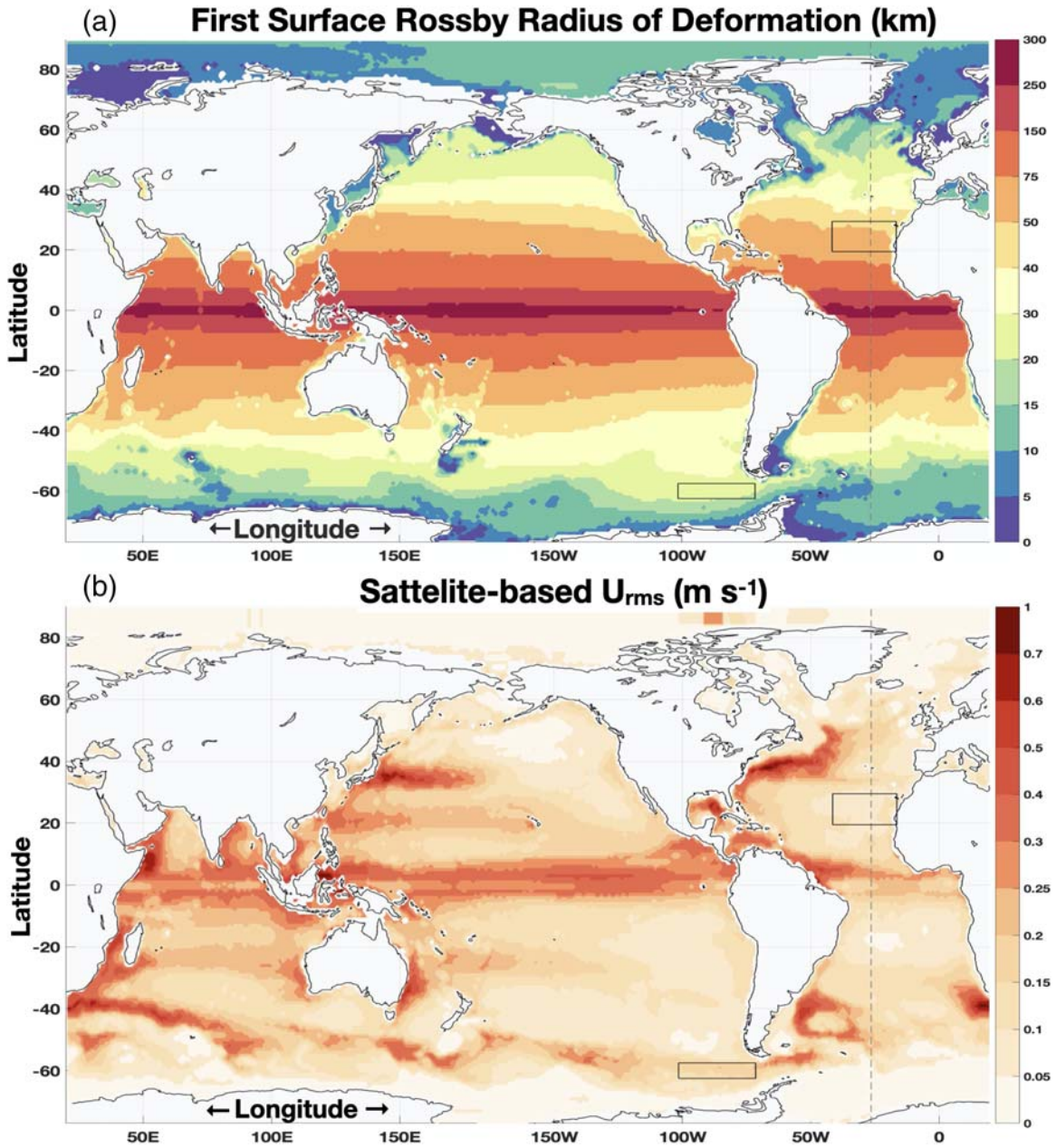

Figure A1. The first surface mode deformation radius L_d (a) and the annual mean root mean square (rms) geostrophic eddy velocity u_{rms} derived from sea surface height satellite data (b).

geostrophic equations in the equatorial band (Lagerloef et al., 1999). The u_{rms} is defined here as the root mean square of the mean EKE, computed from the altimetric geostrophic velocity anomalies over the period 1 January 1993 to 15 May 2017 and is regridded onto the WOA grid before computing u_{rms} (Figure A1b).

Current meter data are used in the East (Mooring 4 of ACM04 Garzoli et al., 1996) and West (Mooring 4 of ACM24 Durrieu De Madron & Weatherly, 1994) Atlantic. Both moorings measure velocity at 4 depths ranging 900 to 3,915 m for ACM24 and from 210 to 4,092 m for ACM04. The first EOF of the measured EKE explains 84% and 90% of the variance for AMC24 and AMC04, respectively. The modes are linearly interpolated to the surface and normalized with the surface value. The results are interpreted as an indication that we find similar behavior from observations of ocean currents as from rough-bottom modes derived using surface modes.

Appendix B: Solving for Φ and L_d

The linear Quasi Geostrophic Potential Vorticity equation governs flows with small Rossby numbers. Assuming a plane wave solutions of the form $\sim \phi(z)\tilde{\Psi}e^{(ikx+iyl-i\omega t)}$ yields a differential equation for the vertical structure the horizontal flow $\phi(z)$ (Gill, 1982; Pedlosky, 1987; Wunsch, 2015):

$$\frac{d}{dz}\left(\frac{f_0^2}{N^2}\frac{d\phi}{dz}\right)+\frac{1}{c^2}\phi=0,\ \text{with}\ N^2(z)=g\left(\alpha\frac{\partial\Theta}{\partial z}-\beta\frac{\partial S_A}{\partial z}\right). \tag{B1}$$

Here $N(z)$ is the buoyancy frequency, and f_0 is the mean Coriolis parameter. Solving the equation requires only climatological (S_A, Θ, p) and boundary conditions. Traditionally, Equation B1 was solved assuming a rigid lid and a flat bottom, such that the vertical velocity $(\partial\phi/\partial z)$ vanishes at the upper and lower boundary $(z = 0, -H)$ (Gill, 1982; Kundu et al., 1975; Nurser & Bacon, 2014; Philander, 1978; Wunsch & Stammer, 1997). However, recent studies argue that bottom topography suppresses the deep flow (de La Lama et al., 2016; LaCasce, 2017), so that it is preferable to solve Equation B1 with no horizontal flow at the bottom instead (i.e., $\phi(z = -H) = 0$). With realistic stratification, Equation B1 is solved numerically using a fourth-order Runge-Kutta step to integrate downward from the surface from an initial guess, with adjustments to the eigenvalue made by using Newton's method until the bottom boundary condition is satisfied. The gravest resulting mode, the "First Surface Mode," resembles the "equivalent-barotropic" structure (Killworth, 1992) in that it decays from the surface to the bottom without changing sign. The surface mode also closely resembles the primary EOF from current meter observations, which often accounts for 50–90% of the variance (de La Lama et al., 2016; LaCasce & Groeskamp, 2020). The deformation radius is then given by Equation 4 (Figure A1a). We also solve Equation B1 for the traditional flat-bottom boundary condition to obtain ϕ_{flat}. We use $|\phi_{\text{flat}}|$, its associated deformation radius, and a new fit of $\gamma^{-1} = 1.38$ days to obtain the flat-bottom estimate of K shown in Figure 1.

Data Availability Statement

WOA18 data can be found in the NOAA website (https://www.nodc.noaa.gov/OC5/woa18/). GSW toolbox can be found online (https://www.teos-10.org/software.htm). For the CMEMS data, go to https://marine.copernicus.eu/, select "data," and use product identifier: *SEALEVEL_GLO_PHY_L4_REP_OBSERVATIONS_008_047*. The mixing output based on this study, for the WOA grid, and related matlab scripts are available online (at https://figshare.com/articles/Groeskamp_et_al_2020_-_mixing_diffusivities/12554555).

Acknowledgments
T. J. Mc. D. gratefully acknowledges support from the Australian Research Council through grant FL150100090, and J. H. L. was supported by the Norwegian Research Council through Project 302743 (The Rough Ocean). Altimetric data analysis was performed using the PANGEO platform, which was supported by NSF Award 1740648. We thank David Marshall and an anonymous reviewer for their insightful comments that improved this paper.

References

Abernathey, R. P., & Marshall, J. (2013). Global surface eddy diffusivities derived from satellite altimetry. *Journal of Geophysical Research: Oceans*, *118*, 901–916. https://doi.org/10.1002/jgrc.20066

Abernathey, R. P., Marshall, J., Mazloff, M., & Shuckburgh, E. (2010). Enhancement of mesoscale eddy stirring at steering levels in the Southern Ocean. *Journal of Physical Oceanography*, *40*(1), 170–184. https://doi.org/10.1175/2009JPO4201.1

Adcroft, A., Anderson, W., Balaji, V., Blanton, C., Bushuk, M., Dufour, C. O., et al. (2019). The GFDL Global Ocean and Sea Ice Model OM4.0: Model description and simulation features. *Journal of Advances in Modeling Earth Systems*, *11*, 3167–3211. https://doi.org/10.1029/2019MS001726

Aoki, K., Kubokawa, A., Sasaki, H., & Sasai, Y. (2009). Midlatitude baroclinic Rossby waves in a high-resolution OGCM simulation. *Journal of Physical Oceanography*, *39*, 2264–2279. https://doi.org/10.1175/2009JPO4137.1

Armi, L., & Stommel, H. (1983). Four views of a portion of the North Atlantic subtropical gyre. *Journal of Physical Oceanography*, *13*(5), 828–857. https://doi.org/10.1175/1520-0485(1983)013<0828:FVOAPO>2.0.CO;2
Barker, P. M., & McDougall, T. J. (2017). Stabilizing hydrographic profiles with minimal change to the water masses. *Journal of Atmospheric and Oceanic Technology*, *34*(9), 1935–1945. https://doi.org/10.1175/JTECH-D-16-0111.1
Barker, P. M., & McDougall, T. J. (2020). Two interpolation methods using multiply-rotated piecewise cubic hermite interpolating polynomials. *Journal of Atmospheric and Oceanic Technology*, *37*(4), 605–619. https://doi.org/10.1175/JTECH-D-19-0211.1
Bretherton, F. P. (1966). Critical layer instability in baroclinic flows. *Quarterly Journal of the Royal Meteorological Society*, *92*(393), 325–334. https://doi.org/10.1002/qj.49709239302
Busecke, J., & Abernathey, R. P. (2019). Ocean mesoscale mixing linked to climate variability. *Science Advances*, *5*(1), eaav5014. https://doi.org/10.1126/sciadv.aav5014
Busecke, J., Gordon, A. L., Li, Z., Bingham, F. M., & Font, J. (2014). Subtropical surface layer salinity budget and the role of mesoscale turbulence. *Journal of Geophysical Research: Oceans*, *119*, 4124–4140. https://doi.org/10.1002/2013JC009715
Canuto, V. M., Cheng, Y., Howard, A. M., & Dubovikov, M. S. (2019). Three-dimensional, space-dependent mesoscale diffusivity: Derivation and implications. *Journal of Physical Oceanography*, *49*(4), 1055–1074. https://doi.org/10.1175/JPO-D-18-0123.1
Chapman, C., & Sallée, J.-B. (2017). Isopycnal mixing suppression by the antarctic circumpolar current and the southern ocean meridional overturning circulation. *Journal of Physical Oceanography*, *47*(8), 2023–2045. https://doi.org/10.1175/JPO-D-16-0263.1
Charney, J. G. (1971). Geostrophic turbulence. *Journal of the Atmospheric Sciences*, *28*(6), 1087–1095. https://doi.org/10.1175/1520-0469(1971)028<1087:GT>2.0.CO;2
Chelton, D. B., deSzoeke, R. A., Schlax, M. G., El Naggar, K., & Siwertz, N. (1998). Geographical variability of the first baroclinic Rossby radius of deformation. *Journal of Physical Oceanography*, *28*(3), 433–460. https://doi.org/10.1175/1520-0485(1998)028<0433:GVOTFB>2.0.CO;2
Chelton, D. B., & Schlax, M. G. (1996). Global observations of oceanic Rossby waves. *Science*, *272*(5259), 234–238.
Cole, S. T., Wortham, C., Kunze, E., & Owens, W. B. (2015). Eddy stirring and horizontal diffusivity from argo float observations: Geographic and depth variability. *Geophysical Research Letters*, *42*, 3989–3997. https://doi.org/10.1002/2015GL063827
de La Lama, M. S., LaCasce, J. H., & Fuhr, H. K. (2016). The vertical structure of ocean eddies. *Dynamics and Statistics of the Climate System*, *1*(1), dzw001. https://doi.org/10.1093/climsys/dzw001
Dewar, W. K. (1986). Mixed layers in gulf stream rings. *Dynamics of Atmospheres and Oceans*, *10*(1), 1–29. https://doi.org/10.1016/0377-0265(86)90007-2
Durrieu De Madron, X., & Weatherly, G. (1994). Circulation, transport and bottom boundary layers of the deep currents in the Brazil Basin. *Journal of Marine Research*, *52*(4), 583–638. https://doi.org/10.1357/0022240943076975
Ferrari, R., & Nikurashin, M. (2010). Suppression of eddy diffusivity across jets in the Southern Ocean. *Journal of Physical Oceanography*, *40*(7), 1501–1519. https://doi.org/10.1175/2010JPO4278.1
Ferreira, D., Marshall, J., & Heimbach, P. (2005). Estimating eddy stresses by fitting dynamics to observations using a residual-mean ocean circulation model and its adjoint. *Journal of Physical Oceanography*, *35*(10), 1891–1910. https://doi.org/10.1175/JPO2785.1
Fox-Kemper, B., Adcroft, A., Böning, C. W., Chassignet, E. P., Curchitser, E., Danabasoglu, G., et al. (2019). Challenges and prospects in ocean circulation models. *Frontiers in Marine Science*, *6*, 65. https://doi.org/10.3389/fmars.2019.00065
Garcia, H. E., Boyer, T. P., Baranova, O. K., Locarnini, R. A., Mishonov, A. V., Grodsky, A., et al. (2019). World ocean atlas 2018: Product documentation. A. Mishonov, Technical Editor.
Garzoli, S. L., Gordon, A. L., Kamenkovich, V., Pillsbury, D., & Duncombe-Rae, C. (1996). Variability and sources of the southeastern Atlantic circulation. *Journal of Marine Research*, *54*(6), 1039–1071.
Gill, A. E. (1982). *Atmosphere-ocean dynamics*. New York: Academic Press.
Gill, A. E., Green, J. S. A., & Simmons, A. J. (1974). Energy partition in the large-scale ocean circulation and the production of mid-ocean eddies. *Deep Sea Research and Oceanographic Abstracts*, *21*(7), 499–528. https://doi.org/10.1016/0011-7471(74)90010-2
Gnanadesikan, A., Pradal, M.-A., & Abernathey, R. (2015). Isopycnal mixing by mesoscale eddies significantly impacts oceanic anthropogenic carbon uptake. *Geophysical Research Letters*, *42*, 4249–4255. https://doi.org/10.1002/2015GL064100
Graham, F. S., & McDougall, T. J. (2013). Quantifying the nonconservative production of conservative temperature, potential temperature, and entropy. *Journal of Physical Oceanography*, *43*(5), 838–862. https://doi.org/10.1175/JPO-D-11-0188.1
Groeskamp, S., Sloyan, B. M., Zika, J. D., & McDougall, T. J. (2017). Mixing inferred from an ocean climatology and surface fluxes. *Journal of Physical Oceanography*, *47*(3), 667–687. https://doi.org/10.1175/JPO-D-16-0125.1
Hallberg, R. (2013). Using a resolution function to regulate parameterizations of oceanic mesoscale eddy effects. *Ocean Modelling*, *72*, 92–103. https://doi.org/10.1016/j.ocemod.2013.08.007
Hautala, S. L. (2018). The abyssal and deep circulation of the Northeast Pacific Basin. *Progress in Oceanography*, *160*, 68–82.
Holloway, G. (1986). Estimation of oceanic eddy transports from satellite altimetry. *Nature*, *323*(6085), 243–244. https://doi.org/10.1038/323243a0
Hunt, F., Tailleux, R., & Hirschi, J. (2012). The vertical structure of oceanic Rossby waves: A comparison of high-resolution model data to theoretical vertical structures. *Ocean Science*, *8*, 19–35. https://doi.org/10.5194/os-8-19-2012
IOC, SCOR, & IAPSO (2010). The international thermodynamic equation of seawater—2010: Calculation and use of thermodynamic properties. Intergovernmental Oceanographic Commission, Manuals and Guides. UNESCO (English), [Available online at www.TEOS-10.org].
Jackett, D. R., & McDougall, T. J. (1997). A neutral density variable for the world's oceans. *Journal of Physical Oceanography*, *27*(2), 237–263. https://doi.org/10.1175/1520-0485(1997)027<0237:ANDVFT>2.0.CO;2
Jansen, M. F., Adcroft, A., Khani, S., & Kong, H. (2019). Toward an energetically consistent, resolution aware parameterization of ocean mesoscale eddies. *Journal of Advances in Modeling Earth Systems*, *11*, 2844–2860. https://doi.org/10.1029/2019MS001750
Jenkins, W. J. (1987). ^{3}H and ^{3}He in the beta triangle: Observations of gyre ventilation and oxygen utilization rates. *Journal of Physical Oceanography*, *17*(6), 763–783. https://doi.org/10.1175/1520-0485(1987)017<0763:AITBTO>2.0.CO;2
Jenkins, W. J. (1998). Studying subtropical thermocline ventilation and circulation using tritium and ^{3}He. *Journal of Geophysical Research*, *103*(C8), 15,817–15,831. https://doi.org/10.1029/98JC00141
Jones, C. S., & Abernathey, R. P. (2019). Isopycnal mixing controls deep ocean ventilation. *Geophysical Research Letters*, *46*, 13,144–13,151. https://doi.org/10.1029/2019GL085208
Joyce, T. M., Luyten, J. R., Kubryakov, A., Bahr, F. B., & Pallant, J. S. (1998). Meso- to large-scale structure of subducting water in the subtropical gyre of the eastern North Atlantic Ocean. *Journal of Physical Oceanography*, *28*(1), 40–61. https://doi.org/10.1175/1520-0485(1998)028<0040:MTLSSO>2.0.CO;2

Killworth, P. D. (1992). An equivalent-barotropic mode in the fine resolution antarctic model. *Journal of Physical Oceanography*, *22*(11), 1379–1387. https://doi.org/10.1175/1520-0485(1992)022<1379:AEBMIT>2.0.CO;2
Klocker, A., & Abernathey, R. (2013). Global patterns of mesoscale eddy properties and diffusivities. *Journal of Physical Oceanography*, *44*(3), 1030–1046. https://doi.org/10.1175/JPO-D-13-0159.1
Klocker, A., Ferrari, R., & LaCasce, J. H. (2012). Estimating suppression of eddy mixing by mean flows. *Journal of Physical Oceanography*, *42*(9), 1566–1576. https://doi.org/10.1175/JPO-D-11-0205.1
Klocker, A., & Marshall, D. P. (2014). Advection of baroclinic eddies by depth mean flow. *Geophysical Research Letters*, *41*, 3517–3521. https://doi.org/10.1002/2014GL060001
Kundu, P. K., Allen, J. S., & Smith, R. L. (1975). Modal decomposition of the velocity field near the Oregon Coast. *Journal of Physical Oceanography*, *5*(4), 683–704. https://doi.org/10.1175/1520-0485(1975)005<0683:MDOTVF>2.0.CO;2
LaCasce, J. H. (2017). The prevalence of oceanic surface modes. *Geophysical Research Letters*, *44*, 11,097–11,105. https://doi.org/10.1002/2017GL075430
LaCasce, J. H., Ferrari, R., Marshall, J., Tulloch, R., Balwada, D., & Speer, K. (2014). Float-derived isopycnal diffusivities in the dimes experiment. *Journal of Physical Oceanography*, *44*(2), 764–780. https://doi.org/10.1175/JPO-D-13-0175.1
LaCasce, J. H., & Groeskamp, S. (2020). Baroclinic modes over rough bathymetry and the surface deformation radius. *Journal of Physical Oceanography*, 1–40. https://doi.org/10.1175/JPO-D-20-0055.1
Lagerloef, G. S. E., Mitchum, G. T., Lukas, R. B., & Niiler, P. P. (1999). Tropical pacific near-surface currents estimated from altimeter, wind, and drifter data. *Journal of Geophysical Research*, *104*(C10), 23,313–23,326. https://doi.org/10.1029/1999JC900197
Ledwell, J. R., Watson, A. J., & Law, C. S. (1993). Evidence for slow mixing across the pycnocline from an open-ocean tracer-release experiment. *Nature*, *364*(6439), 701–703. https://doi.org/10.1038/364701a0
Ledwell, J. R., Watson, A. J., & Law, C. S. (1998). Mixing of a tracer in the pycnocline. *Journal of Geophysical Research*, *103*(C10), 21,499–21,529. https://doi.org/10.1029/98JC01738
Marshall, D. P., & Adcroft, A. J. (2010). Parameterization of ocean eddies: Potential vorticity mixing, energetics and Arnold's first stability theorem. *Ocean Modelling*, *32*(3), 188–204. https://doi.org/10.1016/j.ocemod.2010.02.001
McDougall, T. J. (2003). Potential enthalpy: A conservative oceanic variable for evaluating heat content and heat fluxes. *Journal of Physical Oceanography*, *33*(5), 945–963. https://doi.org/10.1175/1520-0485(2003)033<0945:PEACOV>2.0.CO;2
McDougall, T. J., & Barker, P. M. (2011). Getting started with TEOS-10 and the Gibbs Seawater (GSW) Oceanographic Toolbox. SCOR/IAPSO, WG127, ISBN 978-0-646-55621-5.
McDougall, T. J., Jackett, D. R., Millero, F. J., Pawlowicz, R., & Barker, P. M. (2012). A global algorithm for estimating absolute salinity. *Ocean Science*, *8*(6), 1117–1128.
McDougall, T. J., & McIntosh, P. C. (2001). The temporal-residual-mean velocity. Part II: Isopycnal interpretation and the tracer and momentum equations. *Journal of Physical Oceanography*, *31*(5), 1222–1246. https://doi.org/10.1175/1520-0485(2001)031<1222:TTRMVP>2.0.CO;2
Meijers, A. J. S. (2014). The Southern Ocean in the Coupled Model Intercomparison Project Phase 5. *Philosophical transactions. Series A, Mathematical, physical, and engineering sciences*, *372*(2019), 20130296. https://doi.org/10.1098/rsta.2013.0296
Naveira Garabato, A. C., Polzin, K. L., Ferrari, R., Zika, J. D., & Forryan, A. (2015). A microscale view of mixing and overturning across the Antarctic circumpolar current. *Journal of Physical Oceanography*, *46*(1), 233–254. https://doi.org/10.1175/JPO-D-15-0025.1
Nurser, A. J. G., & Bacon, S. (2014). The Rossby radius in the Arctic Ocean. *Ocean Science*, *10*(6), 967–975.
Pedlosky, J. (1987). *Geophysical fluid dynamics*. New York and Berlin: Springer Science & Business Media.
Philander, S. G. H. (1978). Forced oceanic waves. *Reviews of Geophysics*, *16*(1), 15–46. https://doi.org/10.1029/RG016i001p00015
Pradal, M.-A., & Gnanadesikan, A. (2014). How does the Redi parameter for mesoscale mixing impact global climate in an earth system model? *Journal of Advances in Modeling Earth Systems*, *6*, 586–601. https://doi.org/10.1002/2013MS000273
Prandtl, L. (1925). Report on investigation of developed turbulence (Vol. *5*, pp. 136–139).
Pujol, M. I., Faugère, Y., Taburet, G., Dupuy, S., Pelloquin, C., Ablain, M., & Picot, N. (2016). DUACS DT2014: The new multi-mission altimeter data set reprocessed over 20 years. *Ocean Science*, *12*(5), 1067–1090. https://doi.org/10.5194/os-12-1067-2016
Redi, M. H. (1982). Oceanic isopycnal mixing by coordinate rotation. *Journal of Physical Oceanography*, *12*(10), 1154–1158. https://doi.org/10.1175/1520-0485(1982)012<1154:OIMBCR>2.0.CO;2
Rhines, P. (1970). Edge bottom and Rossby waves in a rotating stratified fluid. *Geophysical Fluid Dynamics*, *1*(3-4), 273–302. https://doi.org/10.1080/03091927009365776
Roach, C. J., Balwada, D., & Speer, K. (2018). Global observations of horizontal mixing from Argo float and surface drifter trajectories. *Journal of Geophysical Research: Oceans*, *123*, 4560–4575. https://doi.org/10.1029/2018JC013750
Sijp, W. P., Bates, M., & England, M. H. (2006). Can isopycnal mixing control the stability of the thermohaline circulation in ocean climate models? *Journal of Climate*, *19*(21), 5637–5651. https://doi.org/10.1175/JCLI3890.1
Smith, K. S., & Marshall, J. (2009). Evidence for enhanced eddy mixing at middepth in the Southern Ocean. *Journal of Physical Oceanography*, *39*(1), 50–69. https://doi.org/10.1175/2008JPO3880.1
Spall, M. A., Richardson, P. L., & Price, J. (1993). Advection and eddy mixing in the Mediterranean salt tongue. *Journal of Marine Research*, *51*(4), 797–818. https://doi.org/10.1357/0022240933223882
Stanley, Z., Bachman, S. D., & Grooms, I. (2020). Vertical structure of ocean mesoscale eddies with implications for parameterizations of tracer transport. *Journal of Advances in Modeling Earth Systems*, *12*, e2020MS002151. https://doi.org/10.1029/2020MS002151
Taburet, G., Sanchez-Roman, A., Ballarotta, M., Pujol, M. I., Legeais, J. F., Fournier, F., et al. (2019). DUACS DT2018: 25 years of reprocessed sea level altimetry products. *Ocean Science*, *15*(5), 1207–1224. https://doi.org/10.5194/os-15-1207-2019
Thompson, R. O. R. Y., & Luyten, J. R. (1976). Evidence for bottom-trapped topographic Rossby waves from single moorings. *Deep Sea Research and Oceanographic Abstracts*, *23*(7), 629–635. https://doi.org/10.1016/0011-7471(76)90005-X
Tulloch, R., Ferrari, R., Jahn, O., Klocker, A., LaCasce, J., Ledwell, J. R., et al. (2014). Direct estimate of lateral eddy diffusivity upstream of drake passage. *Journal of Physical Oceanography*, *44*(10), 2593–2616.
Wang, L., Jansen, M., & Abernathey, R. (2016). Eddy phase speeds in a two-layer model of quasigeostrophic baroclinic turbulence with applications to ocean observations. *Journal of Physical Oceanography*, *46*(6), 1963–1985. https://doi.org/10.1175/JPO-D-15-0192.1
Wortham, C., & Wunsch, C. (2014). A multidimensional spectral description of ocean variability. *Journal of Physical Oceanography*, *44*, 944–966. https://doi.org/10.1175/JPO-D-13-0113.1
Wunsch, C. (2015). *Modern observational physical oceanography: Understanding the global ocean*. Princeton: Princeton University Press.
Wunsch, C., & Ferrari, R. (2004). Vertical mixing, energy, and the general circulation of the oceans. *Annual Review of Fluid Mechanics*, *36*(1), 281–314. https://doi.org/10.1146/annurev.fluid.36.050802.122121

Wunsch, C., & Stammer, D. (1997). Atmospheric loading and the oceanic "inverted barometer" effect. *Reviews of Geophysics*, *35*(1), 79–107. https://doi.org/10.1029/96RG03037

Zhurbas, V., & Oh, I. S. (2004). Drifter-derived maps of lateral diffusivity in the Pacific and Atlantic Oceans in relation to surface circulation patterns. *Journal of Geophysical Research*, *109*, C05015. https://doi.org/10.1029/2003JC002241

Zika, J. D., & McDougall, T. J. (2008). Vertical and lateral mixing processes deduced from the mediterranean water signature in the North Atlantic. *Journal of Physical Oceanography*, *38*(1), 164–176. https://doi.org/10.1175/2007JPO3507.1

Zika, J. D., McDougall, T. J., & Sloyan, B. M. (2010). Weak mixing in the Eastern North Atlantic: An application of the tracer-contour inverse method. *Journal of Physical Oceanography*, *40*(8), 1881–1893. https://doi.org/10.1175/2010JPO4360.1

Zika, J. D., Sallée, J. B., Meijers, A. J. S., Naveira-Garabato, A. C., Watson, A. J., Messias, M. J., & King, B. A. (2020). Tracking the spread of a passive tracer through southern ocean water masses. *Ocean Science*, *16*(2), 323–336. https://doi.org/10.5194/os-16-323-2020